Applied Catalysis B: Environmental 144 (2014) 538–546

Contents lists available at ScienceDirect

Applied Catalysis B: Environmental

journal homepage: www.elsevier.com/locate/apcatb

Structure–activity relationship of VO_x/CeO_2 nanorod for NO removal with ammonia

Yue Peng, Chizhong Wang, Junhua Li *

State Key Joint Laboratory of Environment Simulation and Pollution Control, School of Environment, Tsinghua University, Beijing 100084, China

ARTICLE INFO

Article history:
Received 2 May 2013
Received in revised form 14 July 2013
Accepted 27 July 2013
Available online 7 August 2013

Keywords:
$DeNO_x$
Vanadia
CeO_2
In situ Raman
FTIR

ABSTRACT

A series of vanadia supported on ceria nanorods are prepared by impregnation method for selective catalytic reduction (SCR) of NO with ammonia. Two kinds of vanadia species (VO_x) (oligomeric and polymeric VO_x) and $CeVO_4$ are dispersed on the ceria surface according to the vanadium surface density. These species slightly suppress the catalyst reducibility and concentration of surface oxygen defects rather than distort the ceria cubic lattice or enlarge the BET surface areas. Polymeric VO_x and CeO_2 create the Lewis acid sites and $CeVO_4$ could be served as the Brønsted acid sites. Polymeric VO_x provide new active sites compared with pure CeO_2 for the SCR reaction and $CeVO_4$ enhance the number of active sites. Moreover, part of the Lewis acid sites might be converted into the Brønsted acid sites at high temperature under the SCR gas flow. According to the investigations of the reaction mechanism, both Lewis and Brønsted acid sites are reactive with gaseous NO. At low temperature, *cis*-$N_2O_2^{2-}$ and dimer $(NO)_2$ are active, while surface nitrite or nitrate species are active at high temperature.

1. Introduction

Supported vanadia are among the most investigated oxidation catalysts for a variety of reactions, such as the SO_2 oxidation or the selective catalytic reduction (SCR) of NO with ammonia, owing to its good surface acidity and oxidation ability. The widely employed catalyst for the SCR reaction is the V_2O_5—WO_3/TiO_2, yielding excellent activity within a narrow temperature range of 300–400 °C [1,2]. However, a full understanding of vanadia species (VO_x) dispersed on supports and the relationship between structure and activity still need to be elucidated. Early studies proposed that the formation of active intermediate species NH_2 was the key step to fulfill the SCR process [2]; or the reaction was divided into two individual cycles: an acid cycle on the V^{5+}—OH groups to capture gaseous NH_3 and a redox cycle on the V=O groups to activate adsorbed NH_3 species [3,4]. With the help of in situ spectroscopy techniques, the investigation of the adsorbed species and surface active sites are remarkably improved. Giakoumelou et al. revealed the structure–activity relationship over the V_2O_5/TiO_2 catalyst, which were related to the surface VO_x densities. By correlating the Raman bands with the reaction details, V—O—V bridge or pairs of adjacent V—O—Ti groups rather than V=O groups could be active during the SCR reaction [5].

Ceria containing materials have been extensively investigated and applied as catalysts or supports for the oxidation reaction or oxidative dehydrogenation (ODH) due to their excellent oxygen storage capacity and reducibility [6–8]. A variety of non-vanadia catalysts, such as CeO_2/TiO_2 [9,10], CeO_2—WO_3 [11] or WO_3/CeO_2—ZrO_2 [12], have been synthesized and measured as model catalysts for the NH_3—SCR reaction. These catalysts exhibited relatively high performance under more widely temperature windows and better resistance to SO_2, H_2O or alkali metal [13,14]. Despite existing efforts to understand the interaction between transition metal (V or Mo) and ceria [7,15–17], the exact molecular structures, surface dispersions and variations of active sites during the SCR reaction have not yet been completely investigated and understood. Bañares et al. extensively investigated the ethane ODH on V^{5+}/CeO_2 catalyst. It appeared that the nature of the active sites, V_2O_5/CeO_2 or $CeVO_4/CeO_2$ for the ethane ODH, were the same on activity or selectivity [18,19]. Whereas some researchers proposed that $CeVO_4$ species were inactive for alkane ODH [20]. Recently, Wu et al. prepared a series of V_2O_5/CeO_2 catalysts and revealed the strong interaction between the defect sites or labile surface oxygen and surface VO_x of ceria. Monomeric, polymeric VO_x to $CeVO_4$ in terms of the V_2O_5 loading were formed on the ceria surface [7].

The objective of this work is to study the structure–activity relationship of VO_x dispersed on CeO_2 nanorod. Furthermore, in situ IR and Raman spectra are employed to reveal the reaction mechanism and active sites during SCR process.

* Corresponding author. Tel.: +86 10 62771093.
E-mail address: lijunhua@tsinghua.edu.cn (J. Li).

0926-3373/$ – see front matter © 2013 Elsevier B.V. All rights reserved.
http://dx.doi.org/10.1016/j.apcatb.2013.07.059

2. Experimental

2.1. Catalyst preparation

CeO_2 nanorods were prepared by hydrothermal, 1.5 g $Ce(NO_3)_3{\cdot}6H_2O$ were dissolved in distilled water and 4 g NaOH were added with vigorous stirring. The mixture was transferred into a Teflon-lined, stainless autoclave at 100 °C for 24 h. The products were collected by filtration and washed several times to remove ionic remnants before being dried at 60 °C and being calcined at 400 °C for 2 h [21,22].

The V_2O_5/CeO_2 catalysts were prepared via the impregnation of CeO_2 nanorods with ammonium metavanadate. Typically, 2 g of CeO_2 were loaded into a 10 mL solution of appropriate amount of ammonium metavanadate and 0.2 g oxalic acid. After continuous stirring for 2 h, the catalyst was filtrated, dried overnight and calcined at 400 °C for 3 h. The catalysts are denoted as V_xCe, where x indicates the theoretical molar ratio of V to Ce.

2.2. SCR performance

Kinetics measurements of SCR performance were performed in a fixed-bed quartz reactor (inner diameter of 5 mm) using 100 mg of catalyst. The feed gas mixture contained 500 ppm NO, 500 ppm NH_3, 3% O_2, 5%H_2O (when used) and the balance was N_2. The total flow rate of the feed gas was 200 $cm^3\ min^{-1}$ and the gas hourly space velocity (GHSV) was approximately 120,000 h^{-1}. The concentrations of the gases (NO, NO_2, N_2O, and NH_3) were continually monitored by an FTIR spectrometer (MultiGas TM 2030 FTIR).

To better evaluate the catalytic activity, kinetic parameters were calculated according to the following equation, applied to the NO conversion:

$$k = -\frac{V}{W} \times \ln(1-x) \quad (1)$$

In the above equation, k is the reaction rate constant ($cm^3\ g^{-1}\ s^{-1}$), V is the total gas flow rate ($cm^3\ s^{-1}$), W is the mass of catalyst in the reactor, and x is the NO conversion in the testing activity. The equation is based on the understanding that the reaction is first order dependent on NO and zero order dependent on NH_3 [1,23]. The apparent activation energy was calculated using the Arrhenius equation, which is given by:

$$k = k_0 e^{-E_a/RT} \quad (2)$$

In the above equation, E_a is the apparent activation energy, and it can be calculated from the slope of the $\ln(k)$ versus $1/T$ curve as the inset.

2.3. Catalyst characterization

Characterization of the BET surface area of the samples was carried out with a Micromeritics ASAP 2020 apparatus. The crystal structure was determined using X-ray diffraction measurements (Rigaku, D/max-2200/PC) between 20° and 80° at a step rate of 10° min^{-1} operating at 40 kV and 30 mA using Cu Kα radiation.

SEM image was graphed with a Helios NanoLab 600i Dual Beam System, FEI Company and TEM image was taken on JEM-2011 LaB6 instrument at a voltage of 200 kV. The samples were prepared by ultrasonic dispersion in ethanol and were dispersed for 8 min, and the transparent suspended droplets were placed on a copper grid using a capillary.

X-ray photoelectron spectroscopy was performed with an ESCALab220i-XL electron spectrometer from VG Scientific using 300 W Al Kα radiations. The binding energies were referenced to the C1s line at 284.8 eV.

Temperature programmed reduction (TPR) experiments were performed on a chemisorption analyzer (Micromeritics, ChemiSorb 2720 TPx) under a 10% H_2/Ar gas flow (50 mL min^{-1}) at a rate of 10 °C min^{-1} up to 650 °C. Each sample was pretreated at 350 °C in He for 1 h before testing. The H_2 consumption of each catalyst preparation was calculated by comparison with that of a standard CuO.

2.4. In situ Raman spectroscopy

In situ Raman spectra were measured using a Raman microscope (InVia Reflex, Renishaw) equipped with a deep-depleted thermoelectrically cooled charge-coupled device array detector and a high-grade Leica microscope. The sample was placed into the sample cell, which is specially designed for catalytic reactions carried out at high temperature and pressure (CCR 1000, Linkam). Catalysts (50 mg) were mounted on unreactive disposable ceramic fabric filters. The 532 nm line (5 mW at sample) of laser was used for recording the Raman spectra. The spectra were recorded by accumulating 20 s at a resolution of ±0.5 cm^{-1}.The sample was pretreated in N_2 at 350 °C for 1 h then was cooled down to room temperature. The gas used for operando was a mixture of 500 ppm NH_3, 500 ppm NO, 3% O_2 and N_2 with a total flow rate of 100 $cm^3\ min^{-1}$. The exhaust gases were introduced to MultiGas TM 2030 FTIR to obtain the SCR activity and Raman spectra simultaneously [24,25].

2.5. In situ DRIFTS

IR spectra were recorded on a Fourier transform infrared spectrometer (FTIR, Nicolet 6700) equipped with a SMART collector and an MCT detector cooled by liquid N_2. Diffuse reflectance measurements were performed in situ in a high temperature cell with a ZnSe window. The catalyst was loaded in the Harrick IR cell and heated to 350 °C under N_2 at a total flow rate of 100 $cm^3\ min^{-1}$ for 1 h to remove any adsorbed impurities. The background spectrum was collected in a flowing N_2 atmosphere and was subtracted from each sample spectrum. The spectra were recorded by accumulating 32 scans at a resolution of 4 cm^{-1}. Here, to diminish the influence of absorbance from different samples, the absorbance intensity was set to 3.00 for every sample at 300 °C.

3. Results and discussion

3.1. SCR performance

The NO conversion of the V_xCe catalysts from 150 to 400 °C is shown in Fig. 1(a), accompanied with the activity of commercial V_2O_5—WO_3/TiO_2 catalyst under the same GHSV. Only the $V_{0.75}$Ce catalyst exhibits higher SCR activity than the V_2O_5—WO_3/TiO_2 below 350 °C, and they both obtain entire NO removal at 350 °C under a GHSV of 120,000 h^{-1}. Above this temperature, the activity of the V_xCe catalysts significantly decline, resulting from the NH_3 oxidation on CeO_2 [26]. N_2 selectivity at 400 °C is calculated (Table 1) and displays the same trending as VO_x loading. It appears that the dispersion of VO_x on CeO_2 promotes not only the NO reduction, but also suppresses the NH_3 oxidation to a certain extent, improving N_2 selectivity.

The SCR activity below 200 °C is further studied to acquire the reactive kinetic information, where the NO conversion is less than 30%. The rate constant, energy barrier and Arrhenius plot are presented in Table 1 and Fig. 1(b), respectively. The rate constant continuously increases with elevating the VO_x loading even when eliminating the influence of the BET surface area. The apparent energy barriers for the $V_{0.35}$Ce and $V_{0.75}$Ce catalysts are significantly lower than those for the V_0Ce and $V_{0.17}$Ce catalysts. It suggests

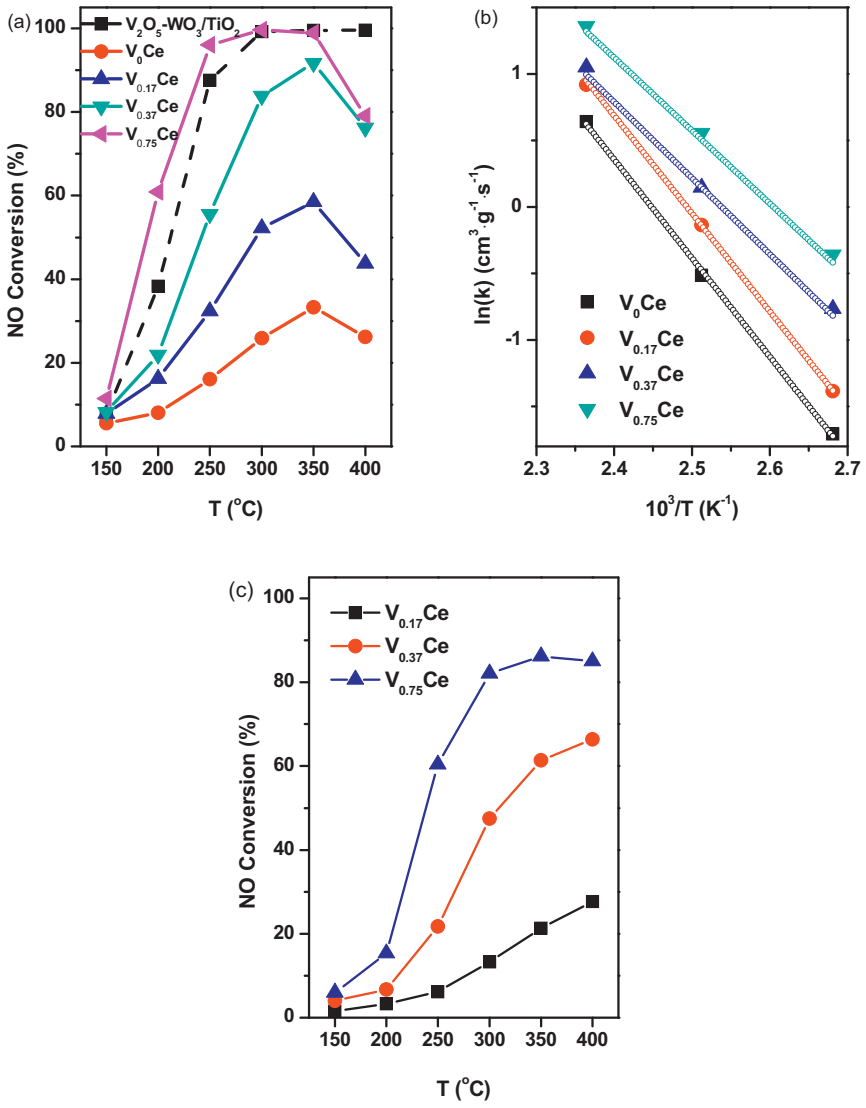

Fig. 1. (a) The NO conversion, (b) Arrhenius plot and (c) the activity under 5% H_2O for the SCR over the V_xCe catalysts. (NO = NH_3 = 500 ppm, O_2 = 3% and balanced by N_2, GHSV = 120,000 h^{-1}).

that the SCR reaction can be remarkably improved by surface vanadium density growing from 3.9 V/nm^2 ($V_{0.17}Ce$) to 8.6 V/nm^2 ($V_{0.35}Ce$). Between the $V_{0.35}Ce$ and $V_{0.75}Ce$, though the rate constant is enhanced, the energy barriers stays nearly unchanged, indicating the style of catalyst active sites formed on the two samples might be the same.

Furthermore, H_2O is as the product of SCR reaction or inevitable existing in the flow gas [1], therefore the SCR activity under H_2O needs to be considered. Fig. 1(c) shows the NO conversion profiles over the vanadium containing catalysts. The existence of H_2O suppressed the SCR activity during the working temperature window. Based on the previous investigation about the influence of H_2O on the traditional V_2O_5/TiO_2 catalysts [1], this inhibition effect could be attributed to the competitive adsorption of H_2O and NH_3 molecules on the acid sites. Moreover, H_2O varied the active sites V_2O_5 to high V cluster, such as $V_{10}O_{28}$ [7], leading to the significantly decrease of surface acidities. While at high temperature (above 400 °C), the influence of H_2O on activity is less important.

Table 1
Physical properties and SCR performance of the V_xCe catalysts.

	S_{BET} (m^2/g)	PV (cc/g)	Dv (nm)	n_s[a] (V/nm^2)	Surface V:Ce[b]	$10^3 \times k/S_{BET}$[c] (cm^3 s^{-1} m^2)	E_a (kJ/mol)	N_2 selectivity[c] (%)
V_0Ce	98.4	0.21	9.52	–	–	1.84	42.0	11.7
$V_{0.17}Ce$	98.7	0.24	9.52	3.9	0.05	2.53	40.1	76.7
$V_{0.37}Ce$	99.6	0.25	9.65	8.6	0.11	4.67	31.5	91.7
$V_{0.75}Ce$	110.3	0.25	9.71	17	0.24	6.34	30.6	95.3

[a] Surface density of vanadium atoms.
[b] Calculated by XPS spectra.
[c] Calculated at 400 °C.

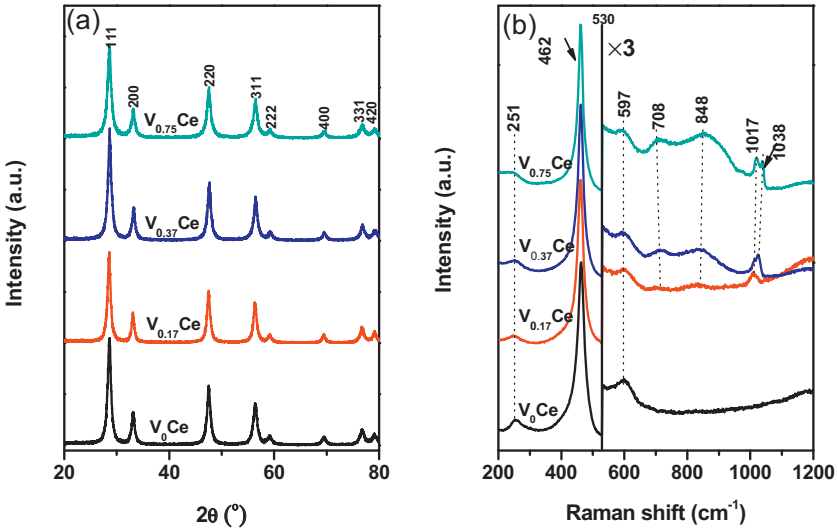

Fig. 2. (a) XRD patterns and (b) dehydration Raman spectra of the V_xCe catalysts.

3.2. Structure characterization

Table 1 summarizes the physical properties of the V_xCe catalysts. The BET surface area, pore volume and particle diameter are nearly unchanged with increasing the VO_x loading. Surface element ratios of V to Ce calculated from the XPS spectra suggest that approximately one third of the vanadium in the impregnated solution is dispersed on the CeO_2 nanorod. Fig. 2(a) presents the XRD profiles of the V_xCe catalysts, only the cubic fluorite ceria phase (PDF# 34-0394) is observed. The intensity of main peaks (28.7°) appears unaffected and the main peak does not move, indicating that the VO_x cannot distort the CeO_2 crystallization or form solid solution of vanadium on CeO_2 cubic fluorite lattice. The VO_x prefer to anchor the surface cerium atoms rather than replacing cerium atoms to produce surface defects.

Dehydrated Raman spectra are employed to characterize the catalyst structure, which are shown in Fig. 2(b). Considering the low intensities of Raman spectra after 530 cm^{-1}, the signals between 530 and 1200 cm^{-1} are magnified by 3 times. The profiles for all the samples are dominated by the peak at 462 cm^{-1}, due to F_{2g} mode of Ce—O vibration with weak bands at 251 and 597 cm^{-1} due to second-order transverse acoustic mode and defect-induced (D) mode, respectively [21,27]. The band intensity ratio ($I_D/I_{F_{2g}}$) of 590 to 464 cm^{-1} is related to the defect sites of ceria-based catalysts, which are summarized in Table 2. Surface defects of catalyst decrease with increasing VO_x loading, indicating that surface VO_x species inhibit the content of defect sites (surface oxygen vacancy) on ceria. Vanadium atom could bond to surface by forming V—O—Ce groups, capping oxygen defect sites and stabilizing the neighboring cerium atoms [7]. Chen et al.'s investigation proposed the similar capping effect. When studied the MoO_3 dispersed on CeO_2, it was found that the accompanying oxygen anions of MoO_3 could cover the oxygen vacancies of CeO_2 (1 1 1) plane [28].

Two broad bands centered at 708 and 848 cm^{-1} occur and are remarkably improved for the $V_{0.75}Ce$ catalyst. These bands can be tentatively assigned to $CeVO_4$, because of the very high surface coverage, 17 V/nm^2, on the $V_{0.75}Ce$ catalyst, which exceeds the theoretical monolayer limitation of amorphous VO_x on CeO_2 (c.a. 9 V/nm^2 for V_2O_5/CeO_2) [18,19]. In addition, one peak at 1017 cm^{-1} is observed on the $V_{0.17}Ce$, attributing to the V=O stretch vibration of oligomeric VO_x. While the peak at 1038 cm^{-1} appear on the $V_{0.37}Ce$, attributing to the V=O stretch vibration of polymeric VO_x [8]. For the $V_{0.75}Ce$ sample, besides the polymeric VO_x, the 1017 cm^{-1} reappears, which might be responsible for the formation of oligomeric VO_x at the expense of large VO_x domain with increasing loading [19]. The surface structures of the catalyst depend on the vanadium density: the surface VO_x are oligomeric for the $V_{0.17}Ce$, polymeric with minor $CeVO_4$ for the $V_{0.37}Ce$ and coexistence of oligomeric, polymeric and $CeVO_4$ for the $V_{0.75}Ce$. Combined with the kinetic result, it is revealed that polymeric VO_x and $CeVO_4$ exhibit relatively low energy barriers and high SCR activity than oligomeric VO_x dispersed on CeO_2.

Fig. 3 shows the SEM and TEM pictures of the CeO_2 nanorods after being calcined for 2 h, most of the CeO_2 can preserve the initial rod morphology and the nanorods were about 300 nm to 2 μm in length. However, some of nanoparticles within 20 nm can also be obtained (shown in Fig. 3(b) and (c)). These could be originated from the broken long nanorods during the thermal treatment.

3.3. Redox properties

Fig. 4 shows the H_2–TPR profiles of the V_xCe catalysts within the range of 300–550 °C. The peak at 482 °C for the V_0Ce is attributed to the reduction of surface Ce^{4+} to Ce^{3+} [6,13]. The peak location moves to high temperature for the vanadia containing catalysts, and the greater vanadium loading corresponds to the higher peak position,

Table 2
Redox properties of the V_xCe catalysts.

	I_{590}/I_{464}[a] (a.u.)	H_2 con (mmol/g_{cat})	H_2 con/S_{BET} (mmol/$m^2{}_{cat}$)	Ce^{3+} ratio[b] (%)	O_α ratio (%)
V_0Ce	1.62	6.14	0.06	–	–
$V_{0.17}Ce$	1.15	6.63	0.07	19.6	47.4
$V_{0.37}Ce$	1.03	9.01	0.09	17.7	43.8
$V_{0.75}Ce$	1.00	12.50	0.11	15.1	37.3

[a] Calculated by intensities of peaks at 464 and 590 cm^{-1} in Fig. 2(b).
[b] Calculated by XPS spectra.

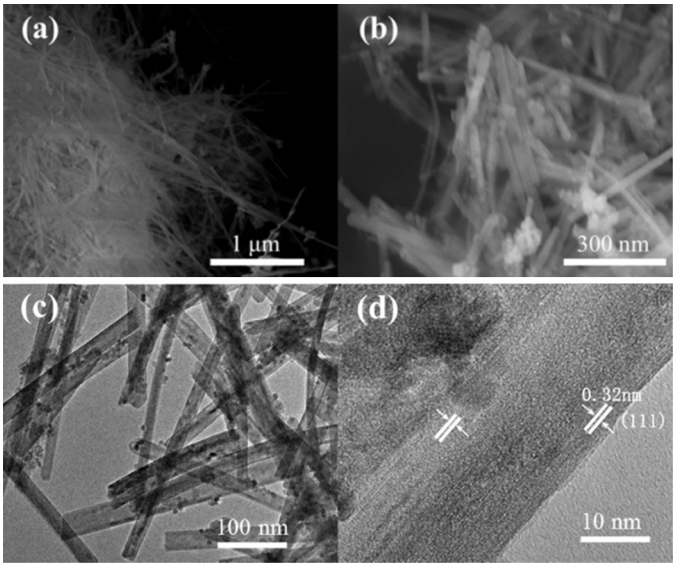

Fig. 3. (a)–(b) SEM and (c)–(d) TEM of the CeO_2 nanorods after being calcined at 400 °C for 2 h.

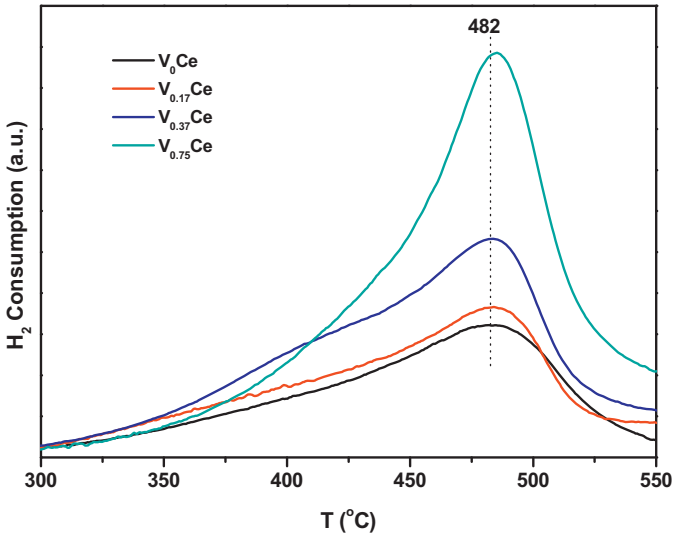

Fig. 4. H_2-TPR profiles of the V_xCe catalysts.

resulting in the low reducibility. Furthermore, the H_2 consumption (Table 2) increases with vanadia loading, indicating the reduction temperatures of VO_x or $CeVO_4$ anchored on CeO_2 are a little higher than the prepared CeO_2. Considering the overlap of reduction temperatures, the reduction peaks cannot be exactly assigned to either surface cerium or vanadium atoms [7].

The XPS spectra of Ce 3d for the V_xCe catalysts are shown in Fig. 5(a). The bands labeled μ, μ'', μ''', ν, ν'' and ν''' represent the $3d^{10}4f^0$ state of Ce^{4+} cations, whereas u' and v' represent the $3d^{10}4f^1$ state, corresponding to Ce^{3+} cations [29]. The spectra of O 1s for the three catalysts are investigated and shown in Fig. 5(b). The O 1s bands can be fitted into two peaks, referred to as the lattice oxygen at 529.3–530.3 eV (O_β) and the surface active oxygen at 530.9–531.9 eV (O_α) [26]. As we know, O_α is highly active in oxidation reactions due to its higher mobility than lattice oxygen O_β. The Ce^{3+} ratios, calculated by $Ce^{3+}/(Ce^{3+}+Ce^{4+})$ and the O_α ratios, calculated by $O_\alpha/(O_\alpha+O_\beta)$ are summarized in Table 2. The results suggest that VO_x species suppress the formation of surface unsaturated Ce^{3+} and labile surface oxygen, and the same trend of $I_D/I_{F_{2g}}$ also be obtained as above. Defect sites and labile surface oxygens both play an essential role in redox properties of ceria containing catalysts [7]. These properties can explain the improvement of N_2 selectivity (low N_2O formed) by vanadia doping.

Moreover, the NO oxidations over the V_xCe catalysts are also employed in the temperature range of 250–400 °C (Fig. 6). The NO_2 yielding decreases with increasing the vanadia loading. The results exhibit good accordance with the TPR and XPS results.

3.4. Surface acidities

It has been established that the catalyst acidity is an important factor for the SCR reaction and the most critical steps are the adsorption and activation of gaseous NH_3 on the catalytic surface. To explore the type, strength and content of surface acid sites, in situ IR spectra of NH_3 adsorption/desorption are employed. Fig. 7 shows the NH_3 adsorption on the V_xCe catalysts at 100 °C. All the spectra present NH_3 adsorption bands at similar positions. Bands within the range of 1100–1300 cm^{-1} and a weak peak centered at 1560 cm^{-1} can be assigned to the ν_s and ν_{as} modes of the N—H bonds in NH_3 linked to Lewis acid sites, while bands at 1440 and 1610 cm^{-1} are

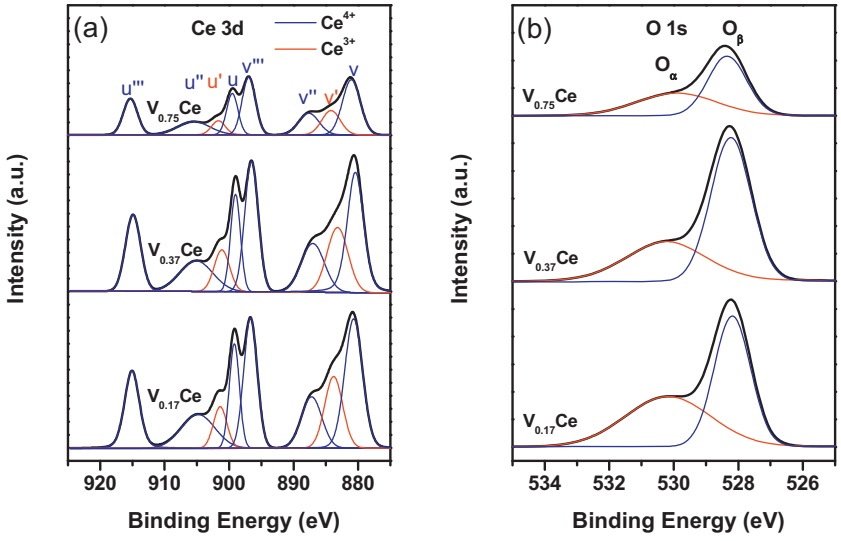

Fig. 5. XPS spectra of (a) Ce 3d and (b) O 1s over the V_xCe catalysts.

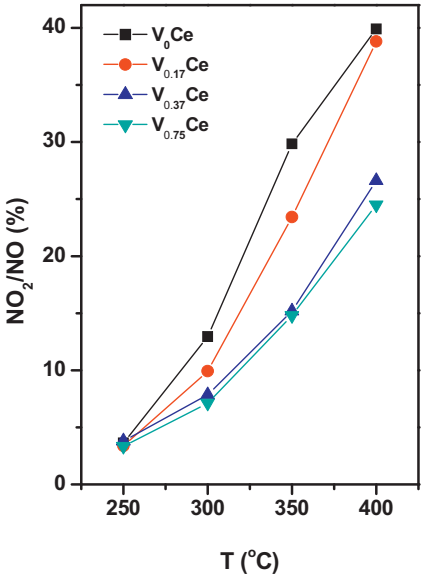

Fig. 6. NO oxidation over the V_xCe catalysts measured at 250–400 °C (NO = 500 ppm, O_2 = 3% and balanced by N_2, GHSV = 120,000 h^{-1}.

Table 3
Surface acidities of the V_xCe catalysts.

	Lewis acidity[a] (a.u.)	Brønsted acidity (a.u.)	Total acidity (a.u.)
V_0Ce	13.25	1.67	14.92
$V_{0.17}Ce$	13.61	3.34	16.95
$V_{0.37}Ce$	29.87	4.58	34.43
$V_{0.75}Ce$	32.14	11.26	43.40

[a] Calculated by the IR of NH_3 adsorption at 100 °C.

due to the ν_{as} and ν_s modes, respectively, of NH_4^+ chemisorbed on Brønsted acid sites [23,30]. Bands centered at 1150 and 1440 cm^{-1} are employed for the quantity of the Lewis and Brønsted acid sites, their integral peak areas represent the corresponding acidities, and the results are summarized in Table 3. Without vanadia, CeO_2 exhibits certain Lewis acid sites and little Brønsted acid sites. When vanadia is dispersed on, both the Lewis and Brønsted acid sites are promoted. Lewis acid sites are slightly improved on the $V_{0.17}Ce$ compared to the V_0Ce. That suggests vanadia could provide some new adsorption sites, which can be also deduced from IR results: peak at 1121 cm^{-1} is decreased (could be assigned to Lewis acidity on CeO_2) and band at 1155 cm^{-1} is enhanced (could be assigned to Lewis acidity on vanadia). The Lewis acid sites are doubled from $V_{0.17}Ce$ to $V_{0.37}Ce$ and slightly promoted from $V_{0.37}Ce$ to $V_{0.75}Ce$. In terms of the surface V to Ce ratios and Raman peaks assignment, the contribution of Lewis acid sites might be provided by both CeO_2 and polymeric VO_x. For the Brønsted acid sites, the remarkable promotion in quantity (doubled) is merely observed from $V_{0.37}Ce$ to $V_{0.75}Ce$, resulting from the large loading of $CeVO_4$. Compared with the Arrhenius plot (energy barriers changes from $V_{0.17}Ce$ to $V_{0.37}Ce$ and rate constant increases from $V_{0.37}Ce$ to $V_{0.75}Ce$), the Lewis acid sites from polymeric VO_x decreases the energies barriers, that is, generating new active sites; the Brønsted acid sites from $CeVO_4$ increases the reaction activity, that is, improving the number of active sites.

To investigate NH_3 desorption bahaviors, IR spectra are employed over the $V_{0.75}Ce$ catalyst (Fig. 7(b)) in the temperature range of 100–350 °C. The catalyst pretreated under 500 ppm NH_3 is purged in N_2 at 100 °C for 1 h to remove weakly physisorbed NH_3 [31]. Both Lewis and Brønsted acid sites diminish with elevating the temperature. Brønsted acid sites decreases at 250 °C, while Lewis acid sites are still observable above 300 °C. It appears that the stability of Lewis acid sites is stronger than that of Brønsted acid sites under thermal treatment on the $V_{0.75}Ce$.

3.5. Reaction mechanism

Extensive studies on SCR reaction mechanism is carried out by in situ IR spectra over the $V_{0.75}Ce$ catalysts at 150, 250 and 350 °C, respectively (Fig. 8). First, the sample pretreated in N_2 at 350 °C is purged by 500 ppm NH_3 for 1 h at 150 °C and then is induced by N_2 for another 30 min to remove physical adsorbed NH_3. Both Lewis (1167 cm^{-1}) and Brønsted (1427 and 1657 cm^{-1}) acid sites are obtained. After NO and O_2 pass over the sample, adsorbed NH_3 species weakens and disappears within 10 min, while some new peaks occurs, locating at 1248, 1367, 1431, 1570 and 1692 cm^{-1}. These peaks can be assigned to bridging nitrate (1248 and 1570 cm^{-1}), monodentate nitrite (1431 cm^{-1}) as well as *cis*-$N_2O_2^{2-}$ on ceria (1367 cm^{-1}) and dimer $(NO)_2$ (1692 cm^{-1}) on vanadia groups [29,30,32]. Nolan investigated the NO adsorption on ceria by DFT calculation and proposed that two NO molecules could form a strong adsorption at neighboring vacancy sites as a N—N-like bond (that is, *cis*-$N_2O_2^{2-}$), and this adsorption might be suppressed at the doped ceria surfaces [33]. When the gaseous

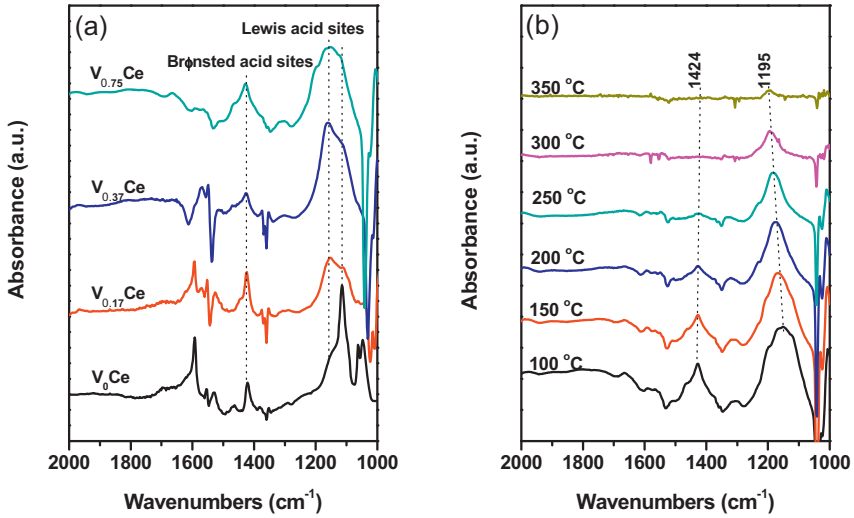

Fig. 7. In situ IR spectra of (a) NH_3 adsorption on the V_xCe catalysts measured at 100 °C and (b) NH_3 desorption on $V_{0.75}Ce$ measured at 100–350 °C.

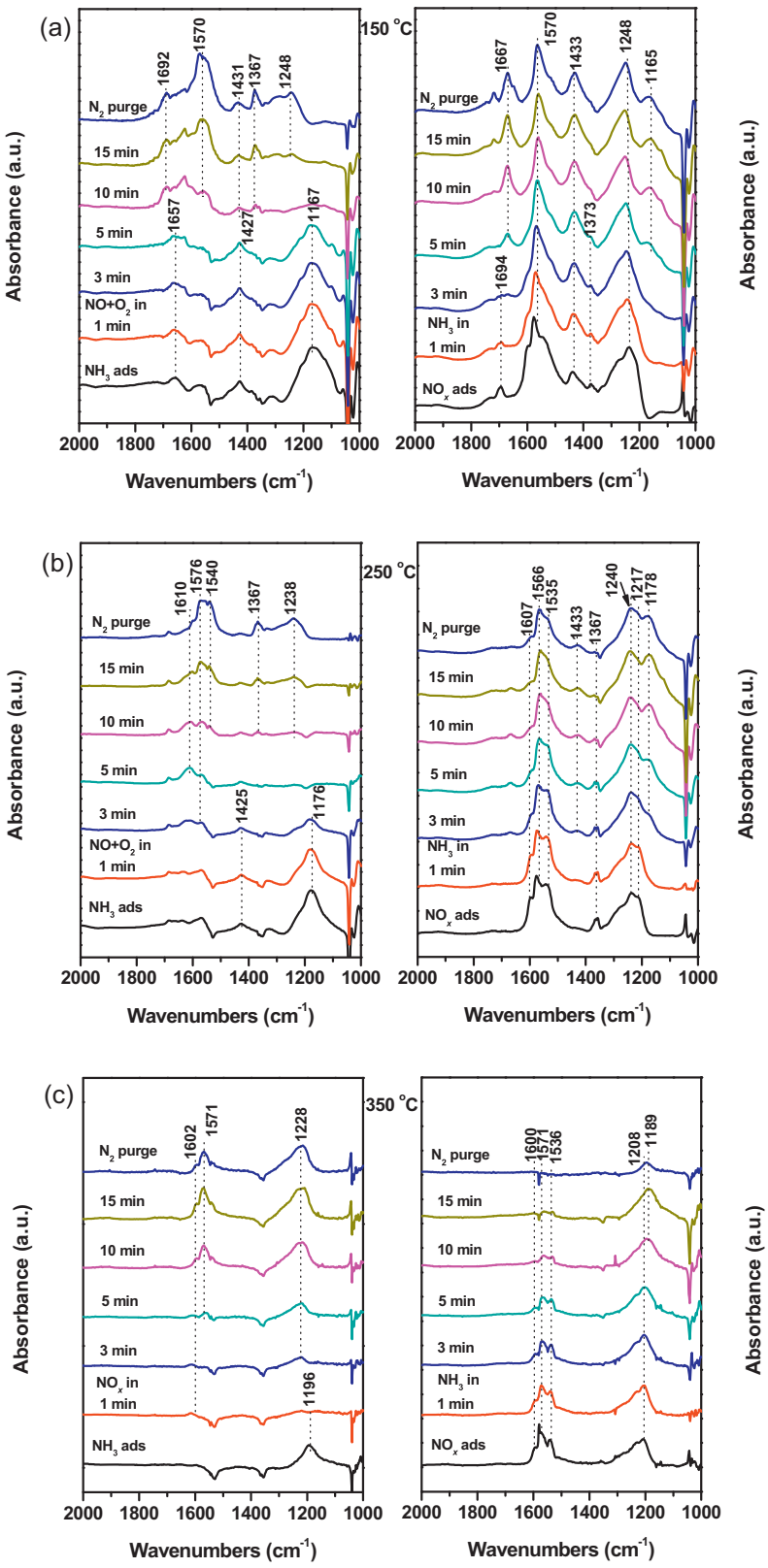

Fig. 8. Sequential IR spectra of $V_{0.75}Ce$ recorded under various atmospheres: the dehydrated catalyst was first treated by NH_3, then NO + O_2 was added, and finally the NO + O_2 was stopped and the reversed order at (a) 150, (b) 250 and (c) 350 °C.

order is reversed, the four species (nitrate, nitrite, *cis*-$N_2O_2^{2-}$ and dimer $(NO)_2$) cover the catalysts after introducing NO and O_2. As soon as NH_3 is passed into, the weak peaks at 1373 and 1694 cm^{-1} decrease and nearly disappear after 3 min, indicating *cis*-$N_2O_2^{2-}$ and dimer $(NO)_2$ can both react with NH_3 species at 150 °C. The peaks attributed to nitrite and nitrate stay unchanged even after 15 min during NH_3 or N_2 purging. The results indicate that Lewis and Brønsted acid sites are involved in the SCR reaction at low temperature, *cis*-$N_2O_2^{2-}$ and dimer $(NO)_2$ are reactive, while both the bridging nitrate and monodentate nitrite species exhibit inactive.

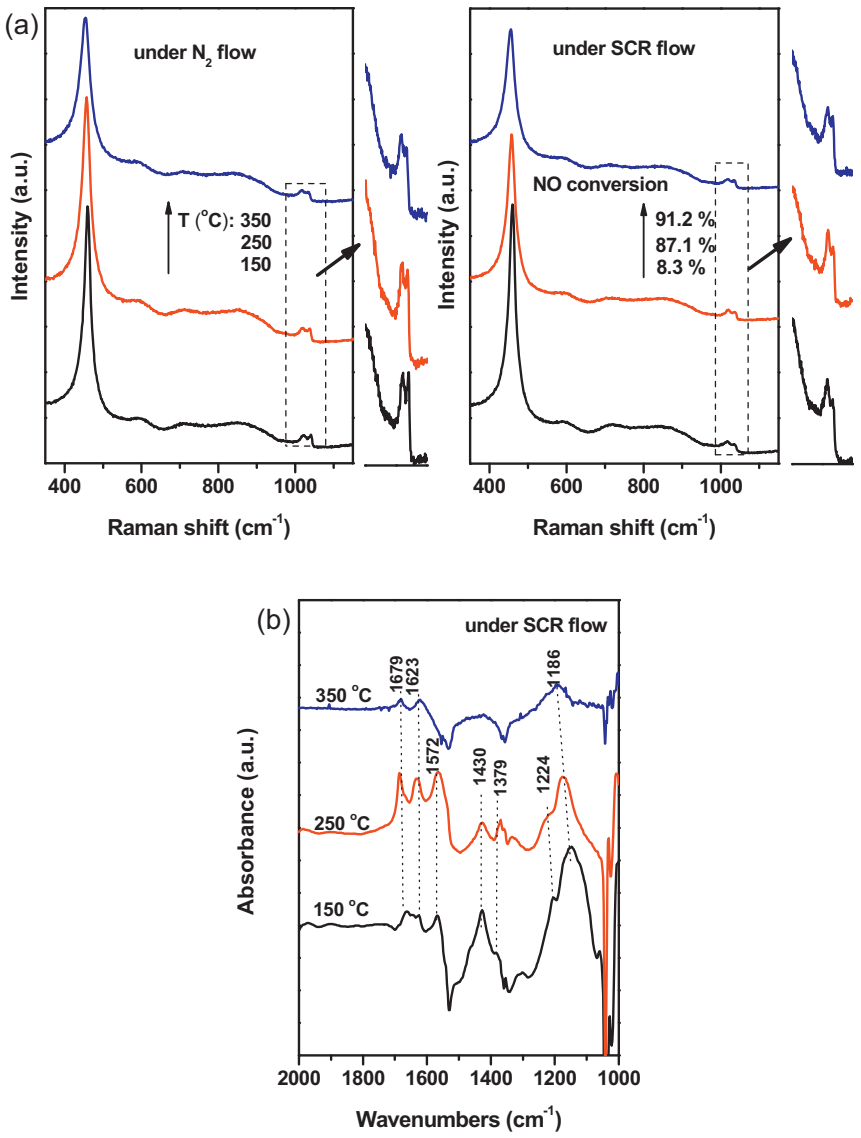

Fig. 9. (a) Operando normalized Raman spectra over $V_{0.75}Ce$ under N_2 and SCR flow and (b) IR spectra under SCR flow measured at 150–350 °C.

Fig. 8(b) shows the spectra at 250 °C. Similar conclusion that both Lewis and Brønsted acid sites involve in the SCR reaction can be obtained, and some new peaks occurs when NO and O_2 are purged over the catalyst. Peaks at 1540 and 1610 cm^{-1} can be attributed to bridging nitrate and adsorbed NO_2, respectively, while peak located at 1540 cm^{-1} can be assigned to bidentate nitrate [30]. After the gas order is reversed, both 1367 and 1607 cm^{-1} decrease. The results indicate that at this temperature, both *cis*-$N_2O_2^{2-}$ and adsorbed NO_2 can take part in the SCR reaction with NH_3 species, while nitrate and nitrite species are still inactive. Fig. 8(c) presents the reaction at 350 °C, only the Lewis acid sites can be detected. Nitrate species and adsorbed NO_2 emerge when NO and O_2 are introduced. All the adsorbed NO_x species decrease when NH_3 is induced into. After 15 min, only Lewis acid sites can be observed on the spectra. The results indicate that at high temperature, even stable bridging nitrate or nitrite species react with NH_3 species.

3.6. Operando study

Finally, operando normalized Raman spectra are recorded under N_2 and reactant flow gas to obtain the information of surface active sites and reaction activity simultaneously (Fig. 9(a)), and the same experiments are carried out again on the IR spectroscopy (Fig. 8(b)). The NO conversion of the $V_{0.75}Ce$ exhibits very similar value as conventional method shown in Fig. 1(b). The intensity of 462 cm^{-1} decreases under N_2 thermal treatment, because the vanadia–ceria catalysts tend to darken and absorb the incident laser light. Polymeric VO_x (1038 cm^{-1}) tend to be consumed (Raman spectra) under SCR flow compared to the spectra under N_2 flow at 150 °C, and the intensity of Lewis acid sites (1160 cm^{-1}) is remarkable on the IR spectra. This expense might be due to the coverage of NH_3 on the Lewis acid sites. At 250 °C, the decrease of polymeric VO_x could be also observed compared to the peak under N_2 treatment and the number of Lewis acid sites on the catalysts significantly decrease. This could be due to the formation of $CeVO_4$ on ceria from polymeric VO_x. Previous studied also found this phase formation from VO_x to $CeVO_4$ on ethane ODH over V^{5+}/CeO_2 catalyst. Based on the operando studies, incipient $CeVO_4$ (amorphous) at the ceria interface region did not influence the activity, selectivity and energy barriers of the catalysts [19]. Correlated with active sites assignment (polymeric VO_x to Lewis acid sites and $CeVO_4$ to Brønsted acid sites), it is possible that part of Lewis acid sites

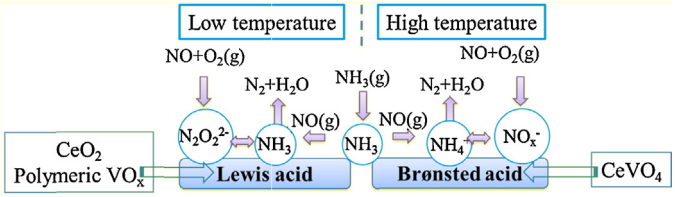

Fig. 10. Structure–activity relationship and reaction mechanism of the vanadia supported on ceria catalysts.

convert into Brønsted acid sites as a result of water adsorption [1,7]. However, this change cannot be observed directly from the IR spectra at 250 °C, resulting from the weak stability of Brønsted acid sites.

The SCR reaction mechanism of the $V_{0.75}Ce$ catalyst is then schemed in Fig. 10. Both Lewis (CeO_2 and polymeric VO_x) and Brønsted ($CeVO_4$) acid sites are reactive. At low temperature, adsorbed *cis*-$N_2O_2^{2-}$ and dimer $(NO)_2$ are active to bond with adsorbed NH_3 species. At high temperature, surface nitrite or nitrate species can also be involved in the reaction.

4. Conclusion

A series of VO_x/CeO_2 nanorods catalysts are prepared by impregnation methods for the selective catalytic reduction of NO with NH_3. Characterization results showed that oligomeric, polymeric VO_x and $CeVO_4$ are formed on the CeO_2 surface according to the surface density of vanadium atoms. These vanadium species do not change the ceria lattice or the BET surface area. Instead, they decrease the catalyst reducibility and surface oxygen defect. Lewis acid sites are mainly originated from CeO_2 and polymeric VO_x while $CeVO_4$ significantly promoted the Brønsted acid sites. By correlating the chemical properties with dynamic data, it appears that Lewis acid sites from polymeric VO_x could generate new active sites compared with ceria and Brønsted acid sites could improve the number of active sites for the SCR reaction.

The studies of the reaction mechanism are carried out over the $V_{0.75}Ce$ catalyst. At low temperature, adsorbed NH_3 could react with *cis*-$N_2O_2^{2-}$ and dimer $(NO)_2$ in spite of the low NO conversion. At high temperature, part of Lewis acid sites convert into Brønsted acid sites and they both exhibit good reactivity, while surface nitrite or nitrate species are also active at 350 °C.

Acknowledgments

The authors gratefully acknowledge the financial support received from the National Natural Science Fund of China (Grant No. 21221004) and the National High-Tech Research and the Development (863) Program of China (2012AA062506) and the Science and Technology Department of Guangdong Province (2011A032303002).

References

[1] G. Busca, L. Lietti, G. Ramis, F. Berti, Appl. Catal. B 18 (1998) 1–36.
[2] G. Ramis, F. Bregani, Appl. Catal. 64 (1990) 259–278.
[3] N.Y. Topsoe, Science 265 (1994) 1217–1219.
[4] N.Y. Topsoe, J. Catal. 151 (1995) 226–240.
[5] I. Giakoumelou, C. Fountzoula, C. Kordulis, S. Boghosian, J. Catal. 239 (2006) 1–12.
[6] Z. Wu, M. Li, S.H. Overbury, J. Catal. 285 (2012) 61–73.
[7] Z. Wu, A.J. Rondinone, I.N. Ivanov, S.H. Overbury, J. Phys. Chem. C 115 (2011) 25368–25378.
[8] Z. Wu, M. Li, S.H. Overbury, ChemCatChem 4 (2012) 1653–1661.
[9] W. Xu, Y. Yu, C. Zhang, H. He, Catal. Commun. 9 (2008) 1453–1457.
[10] B.M. Reddy, A. Khan, Y. Yamada, T. Kobayashi, S. Loridant, J.C. Volta, J. Phys. Chem. B 107 (2003) 5162–5167.
[11] W. Shan, F. Liu, H. He, X. Shi, C. Zhang, Chem. Commun. 47 (2011) 8046–8048.
[12] Y. Li, H. Cheng, D. Li, Y. Qin, Y. Xie, S. Wang, Chem. Commun (2008) 1470–1472.
[13] Y. Peng, J. Li, L. Chen, J. Chen, J. Han, H. Zhang, W. Han, Environ. Sci. Technol. 46 (2012) 2864–2869.
[14] W. Shan, F. Liu, H. He, X. Shi, C. Zhang, Catal. Today 184 (2012) 160–165.
[15] M.A. Bañares, I.E. Wachs, J. Raman Spectrosc. 33 (2002) 359–380.
[16] I.E. Wachs, C.A. Roberts, Chem. Soc. Rev. 39 (2010) 5002–5017.
[17] M. Badlani, I.E. Wachs, Catal. Lett. 75 (2001) 137–149.
[18] M.V. Martinez-Huerta, J. Coronado, M. Fernandez-Garcia, A. Iglesias-Juez, G. Deo, J.L.G. Fierro, M.A. Banares, J. Catal. 225 (2004) 240–248.
[19] M.V. Martinez-Huerta, G. Deo, J.L.G. Fierro, M.A. Bañares, J. Phys. Chem. C 112 (2008) 11441–11447.
[20] W. Daniell, A. Ponchel, S. Kuba, F. Anderle, T. Weingand, D.H. Gregory, H. Knözinger, Top. Catal. 20 (2002) 65–74.
[21] Z. Wu, M. Li, J. Howe, H.M. Meyer, S.H. Overbury, Langmuir 26 (2010) 16595–16606.
[22] K. Zhou, X. Wang, X. Sun, Q. Peng, Y. Li, J. Catal. 229 (2005) 206–212.
[23] G. Qi, R.T. Yang, J. Catal. 217 (2003) 434–441.
[24] G. Tsilomelekis, S. Boghosian, Phys. Chem. Chem. Phys. 14 (2012) 2216–2228.
[25] J. Xu, P. Li, X. Song, C. He, J. Yu, Y. Han, J. Phys. Chem. Lett. 1 (2010) 1648–1654.
[26] M.V. Ganduglia-Pirovano, A. Hofmann, J. Sauer, Surf. Sci. Rep. 62 (2007) 219–270.
[27] A.S. Mamede, E. Payen, P. Grange, G. Poncelet, A. Ion, M. Alifanti, V. Pârvulescu, J. Catal. 223 (2004) 1–12.
[28] X. Du, L. Dong, C. Li, Y. Liang, Y. Chen, Langmuir 15 (1999) 1693–1697.
[29] W. Shan, F. Liu, H. He, X. Shi, C. Zhang, Appl. Catal. B 115–116 (2012) 100–106.
[30] K.I. Hadjiivanov, Catal. Rev. 42 (2000) 71–144.
[31] C. Fang, D. Zhang, L. Shi, R. Gao, H. Li, L. Ye, J. Zhang, Catal. Sci. Technol. 3 (2013) 803–811.
[32] L. Chen, J. Li, M. Ge, L. Ma, H. Chang, Chin. J. Catal. 32 (2011) 836–841.
[33] M. Nolan, J. Phys. Chem. C 112–113 (2009) 2425–2432.